Discovery of novel class 1 phosphatidylinositide 3-kinases (PI3K) fragment inhibitors through structure-based virtual screening

Fabrizio Giordanetto [a,*], Bengt Kull [b], Anita Dellsén [b]

[a] Lead Generation, AstraZeneca R&D Mölndal, Pepparedsleden 1, SE-431 83 Mölndal, Sweden
[b] Bioscience, AstraZeneca R&D Mölndal, Pepparedsleden 1, SE-431 83 Mölndal, Sweden

ARTICLE INFO

ABSTRACT

The discovery of ligand efficient and lipophilicity efficient fragment inhibitors of class 1 phosphatidylinositide 3-kinases (PI3K) is reported. A fragment version of the AstraZeneca compound bank was docked to a homology model of the PI3K p110β isoform. Interaction-based scoring of the predicted binding poses served to further prioritise the virtual fragment hits. Experimental screening confirmed potency for a total of 18 fragment inhibitors, belonging to five different structural classes.

© 2010 Elsevier Ltd. All rights reserved.

Phosphatidylinositide 3-kinases (PI3K) are a family of lipid kinases that play a critical role in signal transduction mechanisms that are of paramount importance to cell regulation and function. Three different classes of PI3Ks (class 1, 2 and 3) have been reported to date. Class 1 PI3Ks phosphorylate the 3′-hydroxy position of the inositol ring of phosphatidylinositide-4,5-biphosphate (PIP$_2$) to produce phosphatidylinositide-3,4,5-triphosphate (PIP$_3$).[1] Class 1 PI3Ks have been subsequently classified into class 1A, comprising the p110α, β and δ catalytic subunits and class 1B (p110γ catalytic subunit). The p110α was the first PI3K identified and several genetic reports demonstrated its relevance to cancer.[2–6] Furthermore, p110α, being activated by the insulin receptor tyrosine kinase, among other receptor-associated kinases, was shown to be involved in insulin signalling and glucose metabolism.[7] The p110β isoform potentiates integrin α_{2b}/β_3 activation and platelet aggregation, and treatment with selective p110β inhibitors markedly decreased arterial thrombosis without a corresponding increase in bleeding time.[8] p110δ and γ impairment has been linked to immunodeficiency and inflammation.[9,10]

During the past decade, structural information on class 1 PI3Ks has greatly improved our understanding of PI3K inhibitors binding and selectivity. The early report on porcine p110γ in its apo and ATP-bound forms confirmed structural similarities between PI3Ks and other known kinases in terms of their catalytic domain fold and ATP binding characteristics.[11] Subsequent studies of porcine p110γ complexed with a variety of early non-specific inhibitors delineated the essential requirements for PI3K inhibition.[12] Recent human p110γ and mouse p110δ co-crystallised with more selective chemical probes[7,13] demonstrated that selectivity for specific class 1 PI3K isoforms could be designed by exploiting differences in the conformational plasticity of the targets, a recurrent theme in selective kinase inhibitor design.[14]

When structural information of a pharmacological target is available, structure-based fragment screening has become a popular strategy to identify ligands interacting with such macromolecule.[15,16] Virtual screening of fragment libraries has also sparked interest,[17–20] as it addresses the limited throughput of biophysical technologies conventionally used in fragment screening.

Based on these premises, our aim was to identify novel p110β fragment inhibitors by using structure-based virtual screening. This resulted in the discovery of 18 ligand efficient and lipophilicity efficient fragment inhibitors belonging to five different structural classes, as reported in the following.

The ultimate goal of the project was to deliver chemical equities inhibiting the p110β isoform for the potential treatment of arterial thrombosis.[8] Furthermore, a certain degree of selectivity towards p110α was desirable in order to minimise the risk for insulin resistance.[7] However, as fragments normally displays low specificity compared to ligands with higher complexity,[21,22] adequate p110β/α and general PI3K selectivity at a fragment level was neither expected nor required. Instead, the focus was to identify efficient p110β fragment inhibitors that would offer opportunities for future optimisation of affinity and selectivity, according to the current PI3K

* Corresponding author. Tel.: +46 31 7065723; fax: +46 31 7763710.
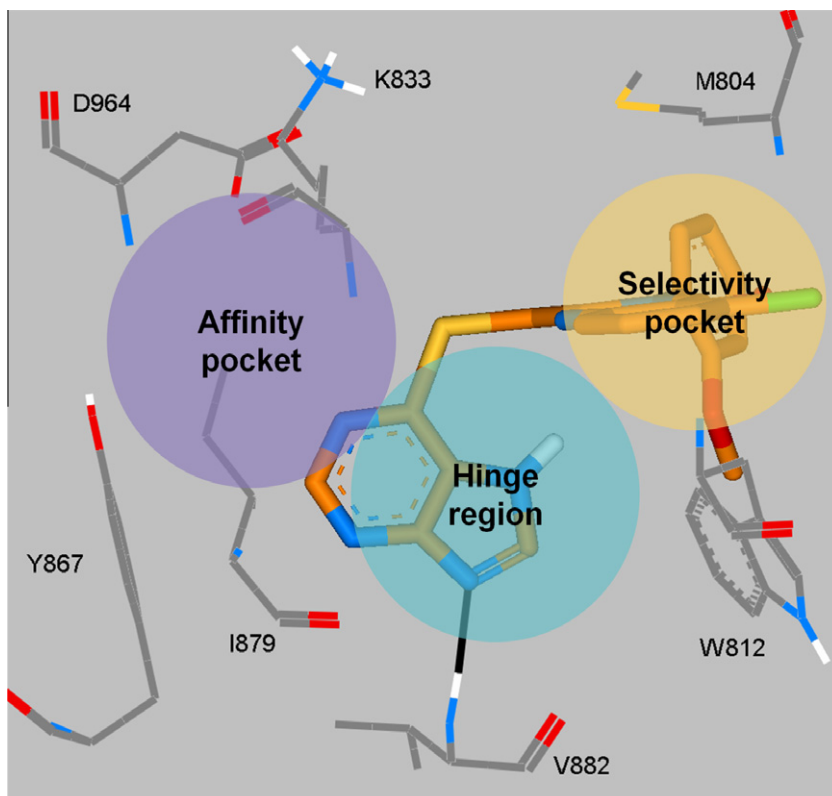   E-mail address: fabrizio.giordanetto@astrazeneca.com (F. Giordanetto).

Figure 1. Structural hypothesis for PI3K inhibition, based on the p110γ–PIK-39 complex (PDB:2CHW).[7] Selected p110γ are displayed as lines, PIK-39 is rendered as sticks (carbon atoms are coloured in orange). Hydrogen bonds are displayed as solid, black lines.

structural evidence[7,11–13] and nonconserved residues across PI3K isoforms. As exemplified in Figure 1, an ideal p110β fragment would thus display (a) effective molecular interactions with the hinge region as a major anchoring point, (b) additional interactions with residues in the affinity pocket to disrupt p110β's catalytic function, (c) available vectors for further substitutions directed at the selectivity pocket and nonconserved amino acids to secure p110β specificity, (d) adequate shape complementarity and filling of the ATP-binding pocket to maximise potency, (e) polar character to minimise optimisation attrition and (f) structure compatible with modular synthetic schemes to allow for straightforward derivatisation.

As an experimental structure of p110β has not been solved yet, a homology model was built using MODELLER[23] based on p110γ complexed with PIK-39 (PDB: 2CHW)[7] and AZD6482 (data not shown) to mimic the conformational rearrangement responsible for p110 isoform specificity.[7]

The fragment library used in the present study consisted of the AstraZeneca collection filtered for ligands with predefined size

(MW ⩽ 300), lipophilicity (c log P ⩽ 3), aromaticity (number of aromatic rings ⩽ 3) and absence of in-house defined structural features.[24] Exhaustive enumeration of tautomeric and protomeric states for the surviving ligands was then carried out with Pipeline Pilot.[25] Three-dimensional structure generation and optimisation was accomplished with Corina[26] and LIGPREP,[27] respectively.

A total of 183,330 unique fragments were docked to the p110β homology model previously described with GLIDE,[28] using the standard precision mode and saving up to 10 poses per fragment. These were further analysed for the occurrence of hydrogen bond interactions with V882, K833 and D964, and hydrophobic contacts with M804, W812, I831, Y867, I879, I881, M953 and I963 (residue numbering according to the p110γ template structure throughout the remainder of the manuscript).

All the fragments satisfying at least two hydrogen bonds with p110β where clustered based on ECFP4[25] and binding poses for cluster representatives were visually inspected to define a final virtual hit list.

Table 1

Descriptive statistics of confirmed PI3K fragment inhibitor hits

	LE[a]	LLE[b]	p110β IC$_{50}$ (µM)[c]	Purity	MW	Log D[d]	C log P[e]
N	18	15	18	15	18	15	18
Min	0.35	3.68	3.6	85%	147	<0	−0.6
Max	0.53	6.98	81.0	98%	257	2.8	3.0
Mean	0.41	5.99	27.5	92%	220	0.52	1.2
CI 95%	0.38–0.43	5.6–6.4	17.5–37.5	89–95%	208–220	0.09–0.95	0.7–1.7

[a] Calculated as −RT ln (IC$_{50}$)/HAC.
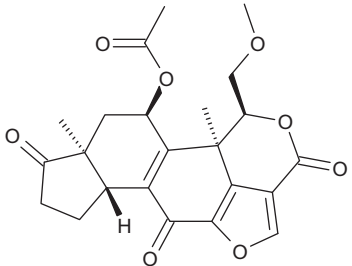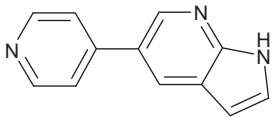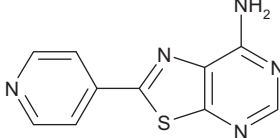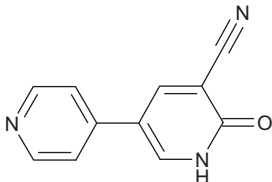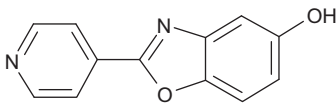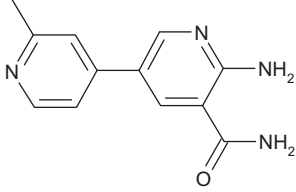
[b] Calculated as pIC$_{50}$ −log D.

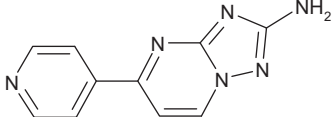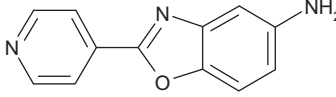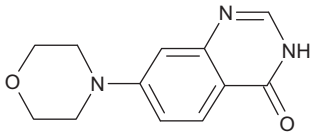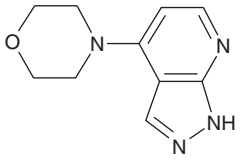[c] Results are mean of at least two experiments. Experimental errors within 20% of value.[29]

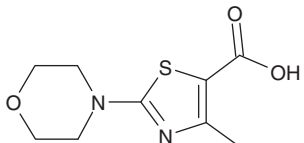[d] Experimental log D using a HPLC method previously described in Ref.[30]

[e] Biobyte C log P™.

F. Giordanetto et al./Bioorg. Med. Chem. Lett. 21 (2011) 829–835

831
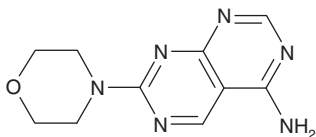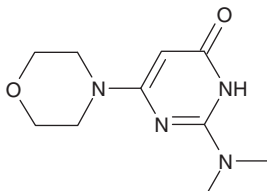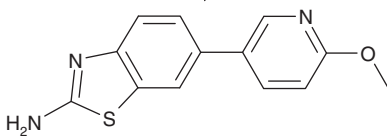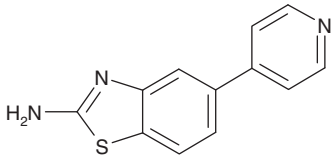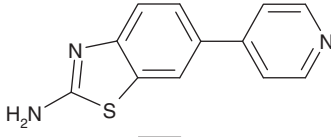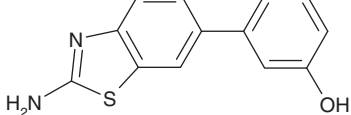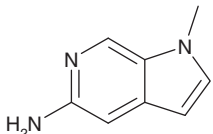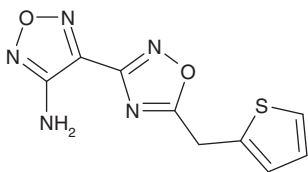
Table 2
p110β potency and PI3K selectivity results for the confirmed fragment inhibitors

Compound	Class	Structure	p110β IC$_{50}$ (μM)[a]	p110α IC$_{50}$ (μM)[a]	p110γ IC$_{50}$ (μM)[a]	p110δ IC$_{50}$ (μM)[a]
Wortmannin			0.015	0.013	0.089	0.004
1	1		17	59	70	40.8
2	1		17	22.7	43.5	11.1
3	1		21	25	>83.3	65.7
4	1		32	83	>83.3	>83.3
5	1		48	ND[b]	ND[b]	ND[b]
6	1		62	>83.3	55.4	43
7	1		81	>83.3	>83.3	>83.3
8	2		5.8	14.2	>83.3	6.4
9	2		17	29.3	>83.3	12

Table 2 (continued)

Compound	Class	Structure	p110β IC$_{50}$ (μM)[a]	p110α IC$_{50}$ (μM)[a]	p110γ IC$_{50}$ (μM)[a]	p110δ IC$_{50}$ (μM)[a]
10	2		17	27.6	>83.3	18
11	2		30	43.2	>83.3	36.8
12	2		34	ND[b]	ND[b]	ND[b]
13	3		3.6	3.6	ND[b]	ND[b]
14	3		4.8	10.2	77	5.1
15	3		9	13	9.7	8.9
16	3		12	10.8	9.1	6.5
17	4		57	ND[b]	ND[b]	ND[b]
18	5		14.2	N/A[c]	N/A[c]	6.8

[a] Results are mean of at least two experiments. Experimental errors within 20% of value.[29]

[b] Not determined.

[c] Not active at highest tested concentration (83.3 μM).

Two hundred and ten fragments were screened for their half-maximal inhibitory concentration (IC$_{50}$) against p110β using an AlphaScreen® competition assay.[29] Eighteen fragments displayed measurable IC$_{50}$'s, yielding a 8.6% hit rate. p110α and general PI3K selectivity was measured with AlphaScreen®[29] on selected fragments. Descriptive statistics for the 18 confirmed fragment hits (frits) are reported in Table 1. Their molecular structures were confirmed by LCMS and sample purity was greater than 85%. The frits

are small (max MW: 257) and relatively polar (CI 95% log D: 0.09–095[30]), thus affording moderately high ligand efficiency (CI 95%: 0.38–0.43) and lipophilicity efficiency (CI 95%: 5.6–6.4), as shown in Table 1.

The 18 frits identified in the present study span 5 different chemical classes, as shown in Table 2. They include pyridines and pyrimidines (class 1, **1**–**7**), morpholines (class 2, **8**–**12**), 1,3-benzothiazol-2-amines (class 3, **13**–**16**), pyrrolo[2,3-c]pyridine (class
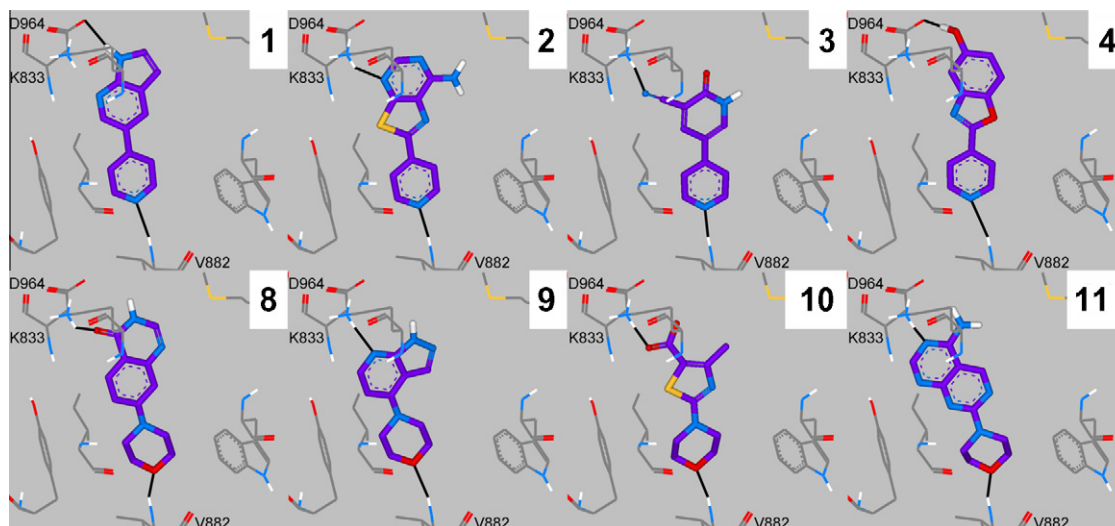
Figure 2. Binding hypothesis for selected pyridine-containing (1st row: **1**–**4**) and morpholine containing (2nd row: **8**–**11**) p110β frits. Selected p110β amino acids are shown as lines. Frits are depicted as sticks (carbon atoms are coloured in purple). Hydrogen bonds are displayed as solid, black lines.

4, **17**) and 1,2,5-oxadiazol-3-amine (class 5, **18**). Class 1 and 2 fragments were predicted to interact with the hinge region of p110β (V882) with their pyridyl nitrogen and morpholine oxygen, respectively, in a similar fashion to previously reported ligands,[7] as displayed in Figure 2. The tendency for morpholine-containing fragments (class 1) to be more potent p110β inhibitors than pyridines (class 2) was not statistically significant ($p = 0.075$). However, morpholines were in general more potent at PI3Kα and PI3Kδ than pyridines ($p = 0.044$ and $p = 0.023$, respectively).

According to the predictions, fragments **1**–**12** establish additional polar interactions with the affinity pocket of p110β (K833, D964) (Fig. 2). Interestingly, this is achieved with several different functional groups: pyrrole (**1**), pyrimidine (**2** and **11**), nitrile (**3**), hydroxyl (**4**), amino (**5**), triazole (**6**), lactam (**8** and **12**), pyridine (**9**), carboxylic acid (**10**), reflecting a wide structural diversity that could be utilised in subsequent modification campaigns (Table 2 and Fig. 2). Here, based on p110β potency considerations alone, the **4** and **7** matched pair suggests that the hydroxyl group should be favoured over the corresponding amino substituent (IC$_{50}$: 32 and 81 μM, respectively) as shown in Table 2.

The predicted hinge-binder motif (class 1: pyridine, class 2: morpholine) is substituted by 5- and 6-membered heterocycles (**3**, **5**, **10** and **12**) as well as different fused ring systems (**1**, **2**, **4**, **6**–**9** and **11**). While the polar character of those rings varies significantly, it is noteworthy that they are all saturated, highlighting specific spatial restraints in the ATP-binding pocket of p110β. More importantly, as several heterocycles are tolerated (**1**–**12**, p110β IC$_{50}$: 5.8–81 μM, Table 2), there could be opportunities to take advantage of their different geometries and corresponding substitution vectors in order to target the specificity pocket responsible for PI3K selectivity,[7,13] and the nonconserved residues that are lining up the purine-binding region. Here, amino acids at position 886, 890 and 950 could be of special interest due to their steric and physicochemical variability across PI3K isoforms. This is of special importance as, in line with expectations, fragments **1**–**12** displayed limited selectivity across different PI3K enzymes, with comparable potencies at p110β, p110α and p110δ but markedly reduced p110γ inhibition ($p < 0.01$), as shown in Table 2. While this finding is hard to rationalise due to the strong amino acid conservation in the hinge binding region of PI3Ks, it suggests opportunities to further explore PI3K selectivity with such chemotype.

The third class of discovered frits comprise 1,3-benzothiazol-2-amines (**13**–**16**) with p110β IC$_{50}$'s in the 3.6–15 μM range (Table 2). All class 3 fragments but **14** were predicted to establish two hydrogen bonds with the hinge region of p110β, utilising both their 2-amino group and benzothiazol nitrogen atom, as displayed in Figure 3. Instead, **14** was predicted to adopt the binding mode already described for class 1 fragments with its pyridyl moiety anchored to the hinge (cf. Figs. 2 and 3). Additional interactions with the affinity pocket were predicted for ether (**13**), pyridine (**15**) and phenol (**16**) functionalities as summarised in Figure 3. Notably, **13** was the most potent p110β inhibitor in this study (IC$_{50}$: 3.6 μM), a result arguably driven by its lipophilicity (log D: 2), the second highest in the set. Compounds **14** and **15** are regioisomers with less than 2-fold difference in p110β potency (IC$_{50}$: 4.8 and 9 μM, respectively). They differ by the position of the pyridyl substituent on the benzothiazole scaffold. Due to steric clash between its 5-(4-pyridyl) substituent and p110β, **14** cannot adopt the 'benzothiazole-hinge' interaction predicted for **15** and other class 3 fragments. However, a 'pyridyl-hinge' interaction predicted for **14** and other class 1 fragments is certainly plausible for **15**, as displayed in Figure 3. In this context, the [1,2,4]triazolo[1,5-*a*]pyridin-2-amine **6** can also be predicted to interact with the hinge similarly to **15**, as depicted in Figure 3. Regardless of the postulated binding pose, the corresponding scaffold hop from [1,2,4]triazolo[1,5-*a*]pyridine to [1,3]benzothiazole resulted in a large potency gain (cf. **6** IC$_{50}$: 62 μM and **14**: 4.8 μM, or **15**: 9 μM).

As fragments **1**–**16** are linear and rigid molecules (max: 2 rotatable bonds) with several hydrogen bond donor/acceptor functionalities at their two ends, it is possible that their ATP-competitive interaction with p110β could result from alternative binding modes, and experimental validation is required to substantiate the present hypotheses.

Compounds **17** and **18** were predicted to interact with the hinge region (2 hydrogen bonds with V882) but not the affinity pocket of p110β (Table 2). Nevertheless, they were selected because they represented interesting p110β inhibition hypotheses. Compound **17** was predicted to be the most effective fragment in filling the bottom of the ATP-binding site of p110β. According to the docking predictions (Fig. 3), its *N*-methyl pyrrole established the best van der Waals contacts with Y867, a critical residue for the PI3K affinity pocket previously described,[7,13] and I879 the notorious gatekeeper
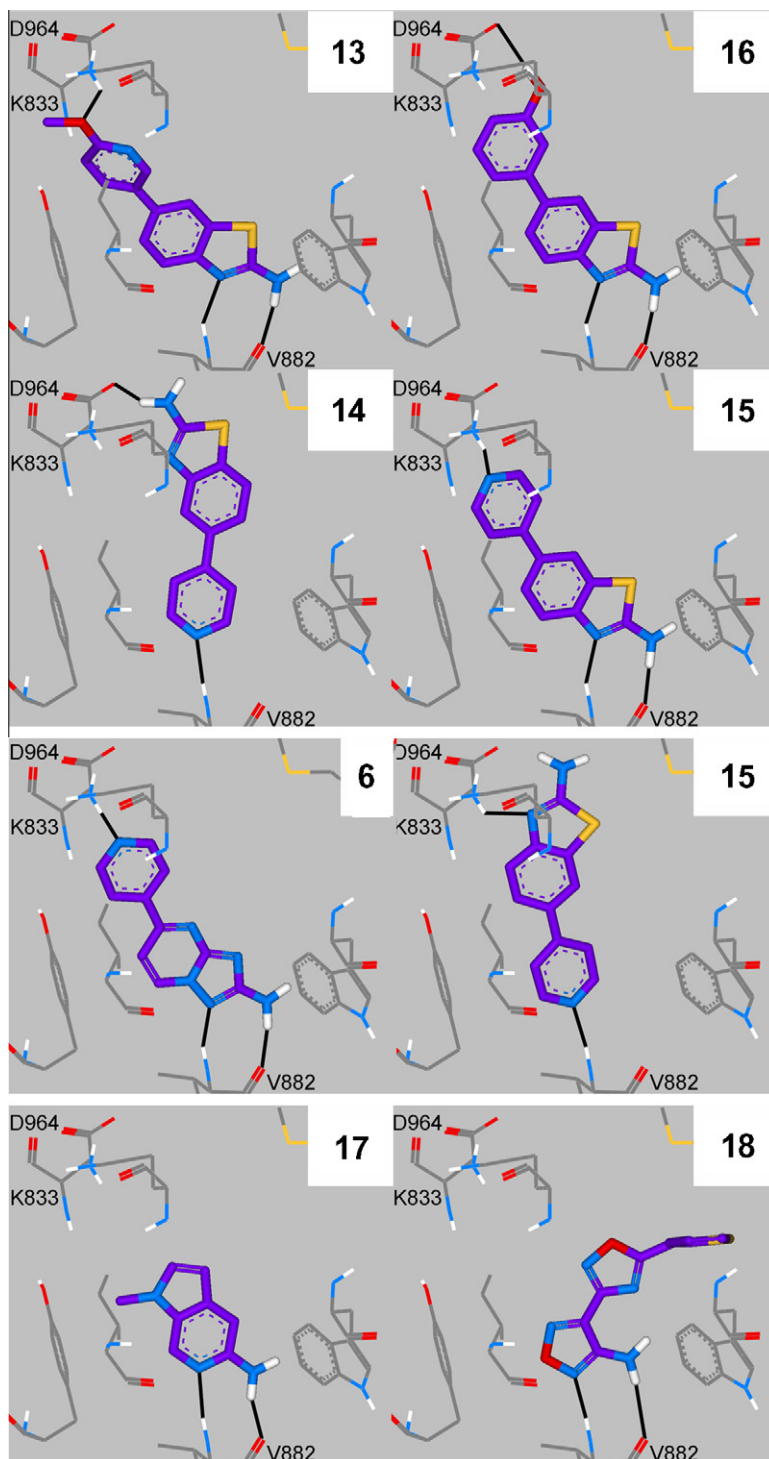
Figure 3. Upper block: binding hypothesis for 1,3-benzothiazol-2-amines frits (**13–16**). Middle block: alternative predicted binding modes for **6** and **15**. Lower block: predicted interactions for **17** and **18**. Selected p110β amino acids are shown as lines. Frits are depicted as sticks (carbon atoms are coloured in purple). Hydrogen bonds are displayed as solid, black lines.

residue that is paramount for kinase sensitivity to small molecule inhibitors.[31–33] Gratifyingly, **17** was the most efficient fragment inhibitor in the set (LE: 0.53, IC$_{50}$: 57 μM, as summarised in Table 2). Compound **18** was the most flexible (3 rotatable bonds) and lipophilic (log D: 2.8) among the active fragments. Based on the docking results, **18** was the only fragment evaluated in this study capable of partially filling the so called PI3K selectivity pocket, which is formed by a conformational rearrangement of M804 at

the entrance of the ATP binding site.[7,13] Accordingly, the thiophene ring of **18** was partly sandwiched by M804 and W812 side chains, as displayed in Figure 3. p110β potency for **18** (IC$_{50}$: 14.2 μM) was disappointing considering its high lipophilicity (LLE: 3.68). However, **18** could be classified as a dual p110β/δ inhibitor (IC$_{50}$: 14.2 and 6.8 μM) with selectivity over the p110α/γ enzymes (no inhibition at 83.3 μM). Based on these results, it is tempting to speculate that the conformational rearrangement observed for p110δ, the

most conformationally flexible of the PI3K isoforms, could be accessible in p110β as well and play a similar role in controlling PI3K selectivity.

In summary, virtual fragment screening against a homology model of p110β identified 18 novel PI3K fragment inhibitors spanning five structural classes with promising ligand and lipophilicity efficiency, laying the foundation for the future optimisation of their p110β potency and PI3K selectivity. These results will be disclosed in a separate account in due course.

References and notes

1. Vanhaesebroeck, B.; Waterfield, M. D. *Exp. Cell Res.* **1999**, *253*, 239.
2. Samuels, Y.; Wang, Z.; Bardelli, A.; Silliman, N.; Ptak, J.; Szabo, S.; Yan, H.; Gazdar, A.; Powell, S. M.; Riggins, G. J.; Willson, J. K.; Markowitz, S.; Kinzler, K. W.; Vogelstein, B.; Velculescu, V. E. *Science* **2004**, *304*, 554.
3. Levine, D. A.; Bogomolniy, F.; Yee, C. J.; Lash, A.; Barakat, R. R.; Borgen, P. I.; Boyd, J. *Clin. Cancer Res.* **2005**, *11*, 2875.
4. Whyte, D. B.; Holbeck, S. L. *Biochem. Biophys. Res. Commun.* **2006**, *340*, 469.
5. Shayesteh, L.; Lu, Y.; Kuo, W. L.; Baldocchi, R.; Godfrey, T.; Collins, C.; Pinkel, D.; Powell, B.; Mills, G. B.; Gray, J. W. *Nat. Genet.* **1999**, *21*, 99.
6. Campbell, I. G.; Russell, S. E.; Choong, D. Y.; Montgomery, K. G.; Ciavarella, M. L.; Hooi, C. S.; Cristiano, B. E.; Pearson, R. B.; Phillips, W. A. *Cancer Res.* **2004**, *64*, 7678.
7. Knight, Z. A.; Gonzalez, B.; Feldman, M. E.; Zunder, E. R.; Goldenberg, D. D.; Williams, O.; Loewith, R.; Stokoe, D.; Balla, A.; Toth, B.; Balla, T.; Weiss, W. A.; Williams, R. L.; Shokat, K. M. *Cell* **2006**, *125*, 733.
8. Jackson, S. P.; Schoenwaelder, S. M.; Goncalves, I.; Nesbitt, W. S.; Yap, C. L.; Wright, C. E.; Kenche, V.; Anderson, K. E.; Dopheide, S. M.; Yuan, Y.; Sturgeon, S. A.; Prabaharan, H.; Thompson, P. E.; Smith, G. E.; Shepherd, P. R.; Daniele, N.; Kulkarni, S.; Abbott, B.; Saylik, D.; Jones, C.; Lu, L.; Giuliano, S.; Hughan, S. C.; Angus, J. A.; Robertson, A. D.; Salem, H. H. *Nat. Med.* **2005**, *11*, 507.
9. Hirsch, E.; Katanaev, V. L.; Garlanda, C.; Azzolino, O.; Pirola, L.; Silengo, L.; Sozzani, S.; Mantovani, A.; Altruda, F.; Wymann, M. P. *Science* **2000**, *287*, 1049.
10. Puri, K. D.; Doggett, T. A.; Douangpanya, J.; Hou, Y.; Tino, W. T.; Wilson, T.; Graf, T.; Clayton, E.; Turner, M.; Hayflick, J. S.; Diacovo, T. G. *Blood* **2004**, *103*, 3448.
11. Walker, E. H.; Perisic, O.; Ried, C.; Stephens, L.; Williams, R. L. *Nature* **1999**, *402*, 313.
12. Walker, E. H.; Pacold, M. E.; Perisic, O.; Stephens, L.; Hawkins, P. T.; Wymann, M. P.; Williams, R. L. *Mol. Cell* **2000**, *6*, 909.
13. Berndt, A.; Miller, S.; Williams, O.; Le, D. D.; Houseman, B. T.; Pacold, J. I.; Gorrec, F.; Hon, W. C.; Liu, Y.; Rommel, C.; Gaillard, P.; Ruckle, T.; Schwarz, M. K.; Shokat, K. M.; Shaw, J. P.; Williams, R. L. *Nat. Chem. Biol.* **2010**, *6*, 117.
14. Schindler, T.; Bornmann, W.; Pellicena, P.; Miller, W. T.; Clarkson, B.; Kuriyan, J. *Science* **2000**, *289*, 1938.
15. Congreve, M.; Chessari, G.; Tisi, D.; Woodhead, A. J. *J. Med. Chem.* **2008**, *51*, 3661.
16. Schulz, M. N.; Hubbard, R. E. *Curr. Opin. Pharmacol.* **2009**, *9*, 1.
17. Macias, A. T.; Foloppe, N.; Chen, I.-J. Abstracts of Papers, 239th National Meeting of the American Chemical Society: San Francisco, CA, 2010; Abstract COMP-84.
18. Xu, Y.; Jansen, H.; Martin, E. Abstracts of Papers, 239th National Meeting of the American Chemical Society: San Francisco, CA, 2010; Abstract CINF-111.
[19]. Feuston, B.; Holloway, M. K.; McGaughey, G.; Culberson, J. C. In *Fragment-Based Drug Discovery*; Zartler, E. R., Shapiro, M. J., Eds.; John Wiley & Sons Ltd: Chichester, 2008; pp 223–244.
20. Teotico, D. G.; Babaoglu, K.; Rocklin, G. J.; Ferreira, R. S.; Giannetti, A. M.; Shoichet, B. K. *Proc. Natl. Acad. Sci. U.S.A.* **2009**, *106*, 7455.
21. Chen, Y.; Shoichet, B. K. *Nat. Chem. Biol.* **2009**, *5*, 358.
22. Barelier, S.; Pons, J.; Gehring, K.; Lancelin, J.-M.; Krimm, I. *J. Med. Chem.* **2010**, *53*, 5256.
23. Marti-Renom, M. A.; Stuart, A.; Fiser, A.; Sánchez, R.; Melo, F.; Sali, A. *Annu. Rev. Biophys. Biomol. Struct.* **2000**, *29*, 291.
24. Davis, A. M.; Keeling, D. J.; Steele, J.; Tomkinson, N. *Curr. Top. Med. Chem.* **2005**, *5*, 421.
25. PIPELINE PILOT, version 7.5. Accelrys, Inc 10188 Telesis Court, Suite 100 San Diego, CA 92121 USA.
26. Gasteiger, J.; Rudolph, C.; Sadowski, J. *Tetrahedron Comput. Methodol.* **1990**, *3*, 537.
27. LIGPREP, version 2.2; Schrödinger, LLC: New York, NY, 2005.
28. GLIDE, version 5.0; Schrödinger, LLC: New York, NY, 2008.
29. Bailey, J. P.; Giles, M. B.; Pass, M. WO2006005914, 2006.
30. Wan, H.; Holmén, A. G. *Comb. Chem. High Throughput Screening* **2009**, *12*, 315.
31. Bishop, A. C.; Ubersax, J. A.; Petsch, D. T.; Matheos, D. P.; Gray, N. S.; Blethrow, J.; Shimizu, E.; Tsien, J. Z.; Schultz, P. G.; Rose, M. D.; Wood, J. L.; Morgan, D. O.; Shokat, K. M. *Nature* **2000**, *407*, 395.
32. Adams, J.; Huang, P.; Patrick, D. *Curr. Opin. Chem. Biol.* **2002**, *6*, 486.
33. Alaimo, P. J.; Kinght, Z. A.; Shokat, K. M. *Bioorg. Med. Chem. Lett.* **2005**, *13*, 2825.